TRENDS IN SCIENCES, 2024; 21(11): 6966 RESEARCH ARTICLE
https://doi.org/10.48048/tis.2024.6966

Entropy Generation in Third-Grade Non-Newtonian Fluid Flow and Heat Transport Through Porous Medium in a Horizontal Channel under Heat Generation

Amala Olkha, Mukesh Kumar* and Rahul Choudhary

Department of Mathematics, University of Rajasthan, Jaipur 302004, India

(* Corresponding author's e-mail: mukeshkumar2011992@gmail.com)

Received: 9 April 2023, *Revised: 14 May 2023*, *Accepted: 21 May 2023*, *Published: 1 October 2024*

Abstract

In this study, entropy production in flow along with heat transport of non-Newtonian fluid via porous medium, is analyzed. For fluid flow via porous medium, a modified Darcy resistance term, is taken in the momentum equation for third-grade fluid. Temperature-dependent viscosity is considered using Vogel's model viscosity. Using adequate transformations, the momentum and heat transport equation are reduced to non-dimensional form and solved analytically invoking homotopy analysis method on MATHEMATICA software. Effects of parameters arising in the study are depicted by graphs on velocity distribution, temperature distribution, and entropy production with Bejan number and discussed. For validity of current findings, the values of velocity and temperature are computed for particular values of the parameters and equated with previously published results, excellent agreement achieved. Furthermore, skin-friction coefficient and Nusselt number values are expressed in tabular form for various values of relevant parameters and discussed. It is noticed that slip parameters (γ) and (β) reduce the entropy generation number (NS). Also noticed that skin friction coefficient upsurges with rising velocity slip parameter (γ) value while, effect of temperature slip parameter (β) is observed to lessen Nusselt number in the absolute sense.

Keywords: Non-Newtonian fluid, Porous medium, Velocity slip, Temperature slip, Entropy production, Bejan number, Homotopy analysis method

Introduction

"All real-life processes are irreversible in nature" [1]. Entropy, a physical quantity described in second law of thermodynamics, is considered as an effective measure of irreversibility in thermodynamic systems. It is experienced that entropy produced in systems reduces the utilization of available work and thus lowers their efficiency. The determination and understanding of the integral ingredients responsible for entropy production is crucial in enhancing the performance of systems. Optimization of energy is the fundamental objective in engineering design of any thermodynamic system. This can be reached by minimization of entropy production in processes. Thus, analysis of entropy production plays a central role in optimization of cost and energy in science and engineering sectors like cooling of electronic devices, heat exchangers, energy storage systems and so on.

Entropy production concept and its minimization in thermal systems was introduced by Bejan [2, 3]. Chauhan and Kumar [4], discussed entropy production in third grade fluid flow using Reynold's model viscosity, in partially filled annulus. Adesanya and Falade [5], discussed entropy production in flow of third grade fluid using regular perturbation method under consideration of Lorentz force impact. Sobamowo and Akinshilo [6], examined 4 grade flow in case of temperature-dependent viscosities taking internal heat generation into account, through a pipe and analysed entropy production. Madhavi *et al.* [7], explored entropy production in a third-grade convection flow from a cylinder applying slip conditions. Madhu *et al.* [8] examined entropy production in third grade fluid flow in a microchannel with variable viscosity and magnetic field impact. They presented numerical solution using finite element method. Zhang *et al.* [9], examined the entropy production in natural convection flow of viscous and non-Newtonian fluids through a L-shaped cavity considering magnetic field impact. Shashikumar *et al.* [10], performed entropy production analysis in inclined microchannel in case of Williamson fluid flow with thermal characteristics. Vyas *et al.* [11], have performed entropy production analysis in Casson fluid flow in a channel with stretchy walls.

Third-grade fluid, a non-Newtonian differential type fluid, is capable to describe the shear thickening and shear thinning phenomena. Such fluids are extensively used in industrial and engineering processes. Therefore, flow of polymers, liquid metals, lubricating oil, and suspensions can be modeled by third-grade fluid and the study of such flow problems have been a subject of extensive research in recent years. The detailed stability analysis of third-grade fluid was presented by Fosdick and Rajagopal [12]. Massoudi and Christie [13], discussed the variable viscosity impacts in case of third-grade fluid flow through a pipe considering viscous dissipation impact. Ariel [14], obtained analytical expressions for flow of such a fluid via a porous channel, whereas Ali *et al.* [15], presented analytical expressions for peristaltic flow through a circular tube. Perturbation solution of third-grade fluid flow in a parallel plates channel was obtained by Yurusoy *et al.* [16]. Slip effects were discussed on steady flow of a third-grade fluid in annular cylinder by Ellahi *et al.* [17]. Heat-mass transport in time dependent flow of third-grade fluid owing to a stretchy surface was examined by Hayat *et al.* [18], incorporating chemical reaction impact. Variable viscosity effects on a third-grade fluid flow over a radiative surface with Arrhenius reaction was discussed by Ogunsola and Peter [19]. Hagen-Poiseuille flow along with heat transport in third-grade flow under influence of variable viscosities and internal heat generation was discussed by Ogunmola *et al.* [20]. Khan *et al.* [21], examined chemical reaction effects on third-grade flow owing to a stretchable surface with variable reactive index and a magnetic field.

The study of flow problems of non-Newtonian fluids via porous medium is important due to several applications of practical importance like, in food processing, manufacturing of ceramics, polymer production, oil recovery, geothermal flow and so forth. Several researchers devoted significant efforts for non-Newtonian fluid flow in porous medium considering various flow configurations. Aksoy and Pakdemirli [22], discussed third-grade flow with modified Darcy's law in a channel via porous medium, and obtained approximate solution. Hayat *et al.* [23], discussed Poiseuille flow of non-Newtonian fluid in a parallel plate channel with permeable walls through porous medium. Baoku *et al.* [24], performed heat-mass transfer analysis of third-grade flow past an upright permeable plate adjacent to a porous medium considering influence of a Lorentz force with partial slip. Prasad *et al.* [25], investigated flow of Jeffrey fluid along with heat transport past a vertical permeable plate adjacent to non-Darcian porous medium using numerical techniques, under assumptions of boundary layer. Akinshilo [26], examined the third-grade fluid flow in porous medium together with heat transport under internal heat generation. Ahmed and Iqbal [27], investigated flow along with heat transport of non-Newtonian power-law fluid using Darcy Brinkman porous medium in

annular sector with a magnetic field. Natural (free) convection in non-Newtonian flow via porous medium with heat source was investigated by Maghsoudi *et al.* [28]. They found that upsurge in value of heat source parameter decreases both velocity and temperature. Further noticed, velocity also decreases with the enhancement in porosity parameter. Rundora and Makinde [29], examined numerically the slip effects on time dependent third-grade flow via porous medium considering influence of Lorentz force. Priyadarsan and Panda [30] explored heat transport in time dependent flow of a 4-grade fluid in a channel in porous medium under consideration of time dependent suction and a magnetic field. Olkha and Dadheech [31, 32], have studied non-Newtonian flow via porous medium owing to permeable stretchy sheet under consideration of Lorentz force impact and analysed entropy production. Olkha and Kumar [33], studied heat and mass transport in Casson fluid flow in a vertical annulus via porous medium. Anasuya and Srinivas [37], have examined viscous 2 fluid flow via porous medium in an inclined channel together with heat transfer characteristics. Maatoug *et al.* [38], have analysed squeezed flow of Jeffery nanofluid in a horizontal channel considering variable chemical species and viscous dissipation impact. Ganjikunta *et al.* [39], have explored non-Newtonian second-grade fluid flow through porous medium influenced by an inclined moving permeable surface considering absorption radiation and chemical reaction. Bafakeeh *et al.* [40], have discussed time dependent rotating flow of second grade fluid via porous medium over an upright plate together with impacts of thermal radiation and chemical reaction. Raghunath and Mohanaramana [41], also investigated time dependent flow of a second grade fluid through porous medium past an inclined plate considering chemical reaction and inclined magnetic field. Deepthi *et al.* [42], have studied heat and mass transport in radiative second grade flow via porous medium along with Hall and ion slip effects, diffusion thermal, and radiation absorption impacts. Kodi and Ravuri [43], performed analysis of heat and mass transport in Kuvshinski fluid flow via porous medium invoking impacts of radiation and inclined magnetic field. Devi and Srinivas [44], have investigated 2 layered flow of non-Newtonian viscoelastic fluid in a vertical channel with porous walls along with heat and mass transport. They assumed pressure gradient to be of oscillatory nature and obtained exact solution utilizing regular perturbation scheme. Kumar *et al.* [45], have performed analysis of flow, heat and mass transfer in Casson nanofluid flow over an exponentially stretching sheet invoking impacts of Lorentz force and heat transfer characteristics. Li *et al.* [46], have studied time dependent squeezed flow of Casson fluid across a horizontal channel via porous medium considering effects of activation energy, chemical reaction and magnetic field. Mixed convection flow of Maxwell nanofluid in a vertical cone via porous medium with varying heat conductivity and Lorentz force impact has been examined by Kodi *et al.* [47].

In aforementioned literature survey we found that there are only a few studies on non-Newtonian flow of grade 3 incorporating entropy production analysis under slip conditions. In this investigation we examined the impact of velocity and temperature slip on flow along with heat transport of a third grade fluid and entropy production. The fluid flow is assumed via porous medium in a parallel-plate horizontal channel under consideration of a heat source. The ruling modeled equations reduced to non-dimensional form under adequate transformations are tackled analytically utilizing homotopy analysis method on MATHEMATICA software. We have used velocity slip boundary condition in this problem because there are non-Newtonian fluids like emulsions, suspensions, polymer melts etc. which exhibit boundary wall slip. Such fluids are significant due to important technological applications, for example, in polymer processing and artificial heart valves polishing. We have used temperature slip condition also. The study is novel due to consideration of entropy production analysis in non-Newtonian third grade fluid flow together with heat transfer and slip boundary condi-

tions. Solution of the problem by homotopy analysis method (HAM) also enhanced novelty of the investigation.

Mathematical formulation

We consider flow of non-Newtonian fluid of third grade via porous medium in an infinite parallel-plate channel. The channel stationary walls are impermeable, and kept at distance h from each other. Cartesian co-ordinate system is considered. We consider $x-$ and $z-$ axes lying in the lower plate, while $y-$ axis perpendicular to it (**Figure 1**). The flow is propelled by applying a pressure gradient (constant) at the entrance of the channel. We have assumed that the channels walls are of infinite length in $x-$ and $z-$ directions. Therefore, all the physical quantities are taken as function of y only.

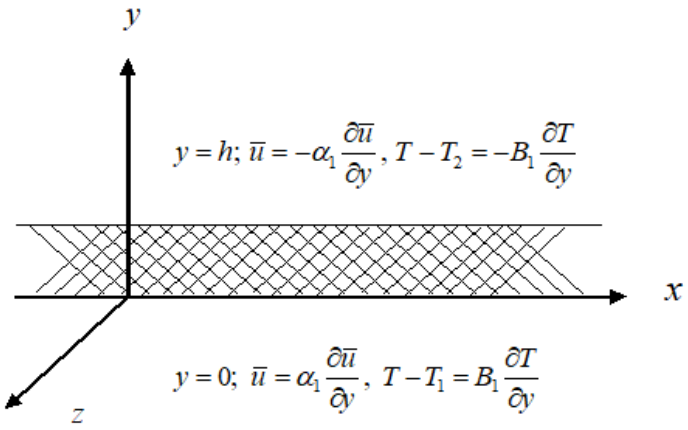

Figure 1: Geometry of the problem.

The governing momentum and energy equation for flow of non-Newtonian fluid of third-grade in porous medium, following Aksoy and Pakdemirli [22], Akinshilo [26], are;

$$\frac{d\bar{\mu}}{dy}\frac{d\bar{u}}{dy}+\bar{\mu}\frac{d^2\bar{u}}{dy^2}+6\beta_3\left(\frac{d\bar{u}}{dy}\right)^2\frac{d^2\bar{u}}{dy^2}-\frac{\phi\bar{u}}{K_1}\left[\bar{\mu}+2\beta_3\left(\frac{d\bar{u}}{dy}\right)^2\right]=\frac{dp}{dx} \tag{1}$$

$$\kappa\frac{d^2T}{dy^2}+\bar{\mu}\left(\frac{d\bar{u}}{dy}\right)^2+2\beta_3\left(\frac{d\bar{u}}{dy}\right)^4+q\,(T-T_1)=0 \tag{2}$$

here $\bar{u}$, the fluid velocity; $\bar{\mu}$, the fluid viscosity; β_3, the non-Newtonian parameter; K_1, porous medium permeability; ϕ, the porosity; p, the pressure; T, the fluid temperature ; T_1, the temperature of the lower plate; κ, represents thermal conductivity and q, represents heat source parameter.

The adequate boundary conditions considered for present problem are;

$$at\,y=0;\ \bar{u}=\alpha_1\frac{d\bar{u}}{dy},\ T-T_1=B_1\frac{dT}{dy} \tag{3}$$

$$at\,y=h;\ \bar{u}=-\alpha_1\frac{d\bar{u}}{dy},\ T-T_2=-B_1\frac{dT}{dy} \tag{4}$$

We take non-dimensional quantities mentioned below;

$$\eta=\frac{y}{h},\quad \mu=\frac{\bar{\mu}}{\mu_0},\quad u=\frac{\bar{u}}{U},\quad \theta=\frac{T-T_1}{T_2-T_1}, \tag{5}$$

Using above the Eqs. (1) and (2) reduce to the following non-dimensional form;

$$\frac{d\mu}{d\eta}\frac{du}{d\eta}+\mu\frac{d^2u}{d\eta^2}+6\beta^*\left(\frac{du}{d\eta}\right)^2\frac{d^2u}{d\eta^2}-Ku\left[\mu+2\beta^*\left(\frac{du}{d\eta}\right)^2\right]=P \tag{6}$$

$$\frac{d^2\theta}{d\eta^2}+\mu\Gamma\left(\frac{du}{d\eta}\right)^2+2\Gamma\beta^*\left(\frac{du}{d\eta}\right)^4+S\theta=0 \tag{7}$$

here U, the reference velocity; μ_0, the reference viscosity; $\beta^*=\frac{\beta_3U^2}{\mu_0h^2}$, the dimensionless third-grade parameter; $K=\frac{\phi}{K_1/h^2}$, the porous medium parameter; $\Gamma=\frac{\mu_0U^2}{\kappa(T_2-T_1)}$, the Brinkman number; T_2, the temperature of the upper plate; $S=\frac{qh^2}{\kappa}$, the non-dimensional parameter of heat source and $P=\frac{h^2}{\mu_0U}\frac{\partial p}{\partial x}$, represents the pressure gradient in non-dimensional form.

The corresponding boundary conditions (3) and (4) are reduced to;

$$at\ \eta=0;\ \ u=\gamma\frac{du}{d\eta},\ \ \theta=\beta\frac{d\theta}{d\eta} \tag{8}$$

$$at\ \eta=1;\ \ u=-\gamma\frac{du}{d\eta},\ \ \theta=1-\beta\frac{d\theta}{d\eta} \tag{9}$$

Where $\gamma=\frac{\alpha_1}{h}$, the slip parameter for velocity; α_1, the velocity slip length; $\beta=\frac{B_1}{h}$, the temperature slip parameter and B_1, the temperature slip length.

For Vogel's model, the viscosity and temperature are related in the following form, (following Massoudi and Christie [13]);

$$\mu=\mu_*\exp\left(\frac{A}{B+\theta}-\theta_w\right), \tag{10}$$

Applying Taylor series Eq. (10) can be written as;

$$\mu=\alpha\left(1-\frac{A\theta}{B^2}\right), \tag{11}$$

here $\alpha=\mu_*\exp\left(A/B-\theta_w\right)$, $\mu_*=\mu_0\exp\left(\theta_w\right)$, A and B are non-dimensional Vogel's viscosity parameters and θ_w, the wall temperature.

Using (11) Eqs. (6)-(7) can be expressed as;

$$-\alpha\frac{A}{B^2}\frac{d\theta}{d\eta}\frac{du}{d\eta}+\left(\alpha-\alpha\frac{A\theta}{B^2}\right)\frac{d^2u}{d\eta^2}+6\beta^*\left(\frac{du}{d\eta}\right)^2\frac{d^2u}{d\eta^2}-Ku\left[\alpha-\alpha\frac{A\theta}{B^2}+2\beta^*\left(\frac{du}{d\eta}\right)^2\right]=P \tag{12}$$

$$\frac{d^2\theta}{d\eta^2}+\Gamma\left(\alpha-\alpha\frac{A\theta}{B^2}\right)\left(\frac{du}{d\eta}\right)^2+2\Gamma\beta^*\left(\frac{du}{d\eta}\right)^4+S\theta=0 \tag{13}$$

Quantities of physical importance

Coefficient of skin-friction

The coefficient of skin-friction at the lower channel wall, $(C_f)_{\eta=0}$ is given by;

$$(C_f)_{\eta=0}=\left[\frac{\tau_{xy}}{(\mu_0U/h)}\right]_{\eta=0}=\left[\mu\frac{du}{d\eta}+2\beta^*\left(\frac{du}{d\eta}\right)^3\right]_{\eta=0} \tag{14}$$

Nusselt Number

The non-dimensional temperature gradient (Nusselt number) at the lower wall is given by;

$$Nu = -\frac{h}{T_2 - T_1}\left(\frac{\partial T}{\partial y}\right)_{y=0} = -\theta'(0) \tag{15}$$

Homotopy analysis method

In this study, we use Liao [34, 35], concept of HAM for the analytical solution of the governing equations. We choose the following initial estimates and auxiliary linear operators for the use of HAM:

$$u_0(\eta) = 0,\ \theta_0(\eta) = \frac{\eta + \beta}{1 + 2\beta}, \tag{16}$$

$$\mathcal{L}_u^* = u'',\ \ \mathcal{L}_\theta^* = \theta'', \tag{17}$$

which fulfil the criteria mentioned below;

$$\mathcal{L}_u^*[C_1 + C_2\,\eta] = 0,\ \ \mathcal{L}_\theta^*[C_3 + C_4\,\eta] = 0 \tag{18}$$

where $C_i (1 \le i \le 4)$ are arbitrary constants, and the zeroth-order deformation equations are given by;

$$(1-s)\mathcal{L}_u^*[u(\eta,s) - u_0(\eta)] = s\hbar_1 \mathcal{N}_u[u(\eta,s),\ \theta(\eta,s)] \tag{19}$$

$$(1-s)\mathcal{L}_\theta^*[\theta(\eta,s) - \theta_0(\eta)] = s\hbar_2 \mathcal{N}_\theta[u(\eta,s),\ \theta(\eta,s)] \tag{20}$$

where $\hbar_1$ and $\hbar_2$ represent nonzero convergence control parameters, and the nonlinear operator $\mathcal{N}_u$ and $\mathcal{N}_\theta$ are defined as;

$$\begin{aligned}\mathcal{N}_u[u(\eta,s),\ \theta(\eta,s)] &= -\frac{\alpha A}{B^2}\frac{du(\eta,s)}{d\eta}\frac{d\theta(\eta,s)}{d\eta} + \alpha\left(1 - \frac{A\theta}{B^2}\right)\frac{d^2u(\eta,s)}{d\eta^2} \\ &+6\beta^*\left(\frac{du(\eta,s)}{d\eta}\right)^2\frac{d^2u(\eta,s)}{d\eta^2} - Ku(\eta,s)\left(\alpha - \frac{\alpha A\theta(\eta,s)}{B^2} + 2\beta^*\left(\frac{du(\eta,s)}{d\eta}\right)^2\right) - P\end{aligned} \tag{21}$$

$$\begin{aligned}\mathcal{N}_\theta[u(\eta,s),\ \theta(\eta,s)] &= \frac{d^2\theta(\eta,s)}{d\eta^2} + \Gamma\alpha\left(1 - \frac{A\theta(\eta,s)}{B^2}\right)\left(\frac{du(\eta,s)}{d\eta}\right)^2 \\ &+ 2\Gamma\beta^*\left(\frac{du(\eta,s)}{d\eta}\right)^4 + S\theta(\eta,s)\end{aligned} \tag{22}$$

where $s \in [0,1]$ is an embedding parameter and the corresponding boundary conditions are given by;

$$u(0,s) = \gamma u'(0,s),\ u(1,s) = -\gamma u'(1,s), \tag{23}$$

$$\theta(0,s) = \beta\theta'(0,s),\ \theta(1,s) = 1 - \beta\theta'(1,s), \tag{24}$$

For $s = 0$ and $s = 1$, we have;

$$u(\eta,0) = u_0(\eta),\ \ u(\eta,1) = u(\eta),\ \theta(\eta,0) = \theta_0(\eta),\ \ \theta(\eta,1) = \theta(\eta) \tag{25}$$

As s varies from 0 to 1, $u(\eta, s)$ varies from initial approximation $u_0(\eta)$ to the required solution $u(\eta)$ of the Eq. (12) and similarly $\theta(\eta, s)$ varies from $\theta_0(\eta)$ to $\theta(\eta)$ as the required solution of Eq. (13). Expanding $u(\eta, s)$ and $\theta(\eta, s)$ in the embedding parameter s, using Taylor's theorem, we can write the following expressions;

$$u(\eta, s) = u_0(\eta) + \sum_{m=1}^{\infty} u_m(\eta) s^m, \tag{26}$$

$$\theta(\eta, s) = \theta_0(\eta) + \sum_{m=1}^{\infty} \theta_m(\eta) s^m, \tag{27}$$

where;

$$u_m(\eta) = \left[\frac{1}{m!}\frac{\partial^m u(\eta, s)}{\partial s^m}\right]_{s=0}, \quad \theta_m(\eta) = \left[\frac{1}{m!}\frac{\partial^m \theta(\eta, s)}{\partial s^m}\right]_{s=0} \tag{28}$$

Auxiliary parameters are mostly responsible for the series' convergence. Assume that the auxiliary parameters ($\hbar_1$ and $\hbar_2$) are chosen so that the series (26)–(27) in converges at $s = 1$, then;

$$f(\eta) = f_0(\eta) + \sum_{m=1}^{\infty} f_m(\eta), \tag{29}$$

$$\theta(\eta) = \theta_0(\eta) + \sum_{m=1}^{\infty} \theta_m(\eta), \tag{30}$$

mth order deformation equation and corresponding boundary conditions are given by;

$$\mathcal{L}_u^*[u_m(\eta) - \varepsilon_m u_{m-1}(\eta)] = \hbar_1 \Im_m^u(\eta), \tag{31}$$

$$\mathcal{L}_\theta^*[\theta_m(\eta) - \varepsilon_m \theta_{m-1}(\eta)] = \hbar_2 \Im_m^\theta(\eta), \tag{32}$$

$$u_m(0) = \gamma {u_m}'(0), \; u_m(1) = -\gamma {u_m}'(1), \; \theta_m(0) = \beta {\theta_m}'(0), \; \theta_m(1) = 1 - \beta {\theta_m}'(1) \tag{33}$$

where;

$$\begin{aligned} \Im_m^u(\eta) = &-\frac{\alpha A}{B^2}\left(\sum_{k=0}^{m-1} u'_{m-1-k}\theta'_k\right) + \alpha\left(u''_{m-1} - \frac{A}{B^2}\left(\sum_{k=0}^{m-1} u''_{m-1-k}\theta_k\right)\right) \\ &-K\left(\alpha u_{m-1} - \frac{\alpha A}{B^2}\left(\sum_{k=0}^{m-1} u_{m-1-k}\theta_k\right) + 2\beta^*\left(\sum_{n=0}^{m-1} u_{m-1-n}\left(\sum_{k=0}^{n} u'_{n-k}u'_k\right)\right)\right) \\ &+6\beta^*\left(\sum_{n=0}^{m-1} u''_{m-1-n}\left(\sum_{k=0}^{n} u'_{n-k}u'_k\right)\right) - P(1-\varepsilon_m) \end{aligned} \tag{34}$$

$$\begin{aligned} \Im_m^\theta(\eta) = \theta''_{m-1} &+ \Gamma\alpha\left(\left(\sum_{k=0}^{m-1} u'_{m-1-k}u'_k\right) - \frac{A}{B^2}\left(\sum_{n=0}^{m-1}\theta_{m-1-n}\left(\sum_{k=0}^{n} u'_{n-k}u'_k\right)\right)\right) \\ &+2\Gamma\beta^*\left(\sum_{n=0}^{m-1}\left(\sum_{i=0}^{n} u'_i u'_{n-i}\right)\left(\sum_{j=0}^{m-1-n} u'_j u'_{m-1-n-j}\right)\right) + S\theta_{m-1} \end{aligned} \tag{35}$$

where $\varepsilon_m = 0, \; if m \leq 1; \; 1, if m > 1$

The general solution of Eqs. (31)-(33) is given by;

$$u_m(\eta) = u_m^*(\eta) + C_1 + C_2\eta \tag{36}$$

$$\theta_m(\eta) = \theta_m^*(\eta) + C_3 + C_4\eta \tag{37}$$

where $u_m^*(\eta)$ and $\theta_m^*(\eta)$ are the particular solutions and $C_i(1 \leq i \leq 4)$ are the constants determined using boundary conditions with the help of the symbolic computation software MATHEMATICA.

Convergence of the HAM solution

According to Liao and Tan [36], the range of the nonzero auxiliary parameter ($\hbar$) has a significant impact on the convergence region and rate of the HAM series. As $\hbar_1$ and $\hbar_2$ are involved in Eqs. (36)–(37), we can expand the HAM solution's convergence zone. To find the appropriate region of $\hbar_1$ and $\hbar_2$, we draw the $\hbar$–curve for 10th, 15th, 20th, 25th, and 30th order approximations (**Figures 2–3**). With the help of these figures, we can easily see that the valid region for $\hbar_1$ is $-2.0 \leq \hbar_1 \leq -0.5$, for $\hbar_2$ is $-2.0 \leq \hbar_2 \leq -0.5$. We can confirm that the solution series (36) and (37) are convergent by selecting values for $\hbar_1$ and $\hbar_2$ in this range.

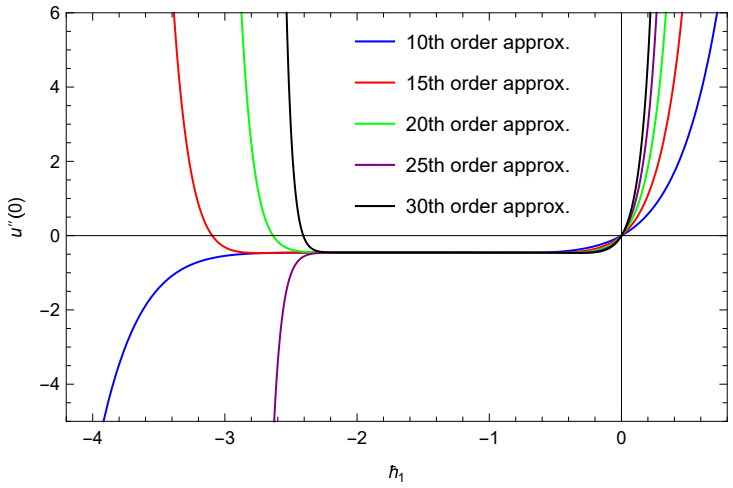

Figure 2: $\hbar_1-$curve for $u''(0)$.

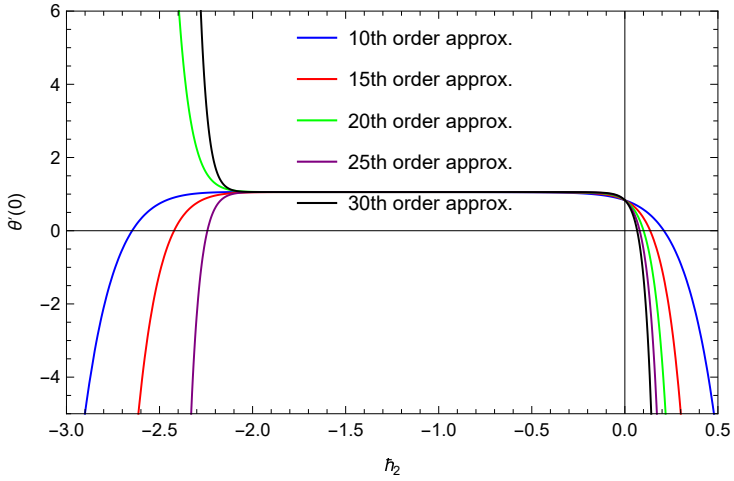

Figure 3: $\hbar_2-$curve for $\theta'(0)$.

Entropy generation

The entropy production in flow field is continuous because of irreversible nature of heat transfer and viscosity effects at the solid boundaries and within the fluid. The dimensional entropy generation within the fluid system is given as;

$$S_{gen} = \frac{\kappa}{T_1^2}\left(\frac{dT}{dy}\right)^2 + \frac{\overline{\mu}}{T_1}\left[\left(\frac{d\bar{u}}{dy}\right)^2\left\{1+\frac{2\beta_3}{\overline{\mu}}\left(\frac{d\bar{u}}{dy}\right)^2\right\} + \frac{\bar{u}^2}{K_1}\left\{1+\frac{2\beta_3}{\overline{\mu}}\left(\frac{d\bar{u}}{dy}\right)^2\right\}\right] \tag{38}$$

here the first and second terms are contributions due to heat transport and fluid friction, respectively.

The non-dimensional entropy production NS is given as;

$$NS = \left(\frac{d\theta}{d\eta}\right)^2 + \Gamma\Omega\left[\mu\left(\frac{du}{d\eta}\right)^2 + +2\beta^*\left(\frac{du}{d\eta}\right)^4 + Ku^2\left\{\mu + 2\beta^*\left(\frac{du}{d\eta}\right)^2\right\}\right] = NS_1 + NS_2 \tag{39}$$

where $NS = \frac{S_{gen}}{\kappa(T_2-T_1)^2/\left(T_1^2h^2\right)}$, the non-dimensional entropy generation rate; $\Omega = \frac{T_1}{T_2-T_1}$, the temperature difference parameter; $NS_1 = \left(\frac{d\theta}{d\eta}\right)^2$, the entropy production number due to heat transport and $NS_2 = \Gamma\Omega\left[\mu\left(\frac{du}{d\eta}\right)^2 + +2\beta^*\left(\frac{du}{d\eta}\right)^4 + Ku^2\left\{\mu + 2\beta^*\left(\frac{du}{d\eta}\right)^2\right\}\right]$, the entropy generation number due to fluid friction. Also the Bejan number (Be) (an irreversibility parameter), defined as;

$$Be = \frac{NS_1}{NS_1 + NS_2}, 0 \le Be \le 1 \tag{40}$$

Results and discussion

The entropy production in steady flow together with heat transport of third-grade fluid via a porous medium in a horizontal channel is explored. The boundary value problem, nonlinear in nature, is solved analytically employing HAM on MATHEMATICA. Profiles of velocity distribution, temperature distribution, entropy production, and Bejan number are sketched for values of various arising parameters taken in ascending order.

Figures 4–8 depict variations in velocity distribution for numerous values of relevant physical parameters. We noticed in **Figure 4** that pace of the flow decreases with upsurging value of third grade parameter (β^*). The reason behind it may be shear thickening nature of the fluid. The impact of slip parameter (γ) for flow is exhibited in **Figure 5**. Influence of γ is observed to upsurge the flow in the entire channel, significantly. With an increase in slip parameter (γ) value pace of the flow close to the wall upsurges which results in increase of velocity field and thus velocity profile improves. **Figure 6** exhibits variation in velocity distribution with porous medium parameter (K). It is observed that fluid flow lessens with increasing value of parameter K. From momentum equation, the Darcy resistance varies inversely as permeability of the porous medium. A smaller permeability causes larger resistance consequently, pace of the flow reduces in the channel. Further, it is seen that upsurge in value of Vogel's viscosity parameter (A) lessens the velocity field, while reverse impact is observed by upsurge in value of Vogel's viscosity parameter (B) as **Figures 7** and **8** depict.

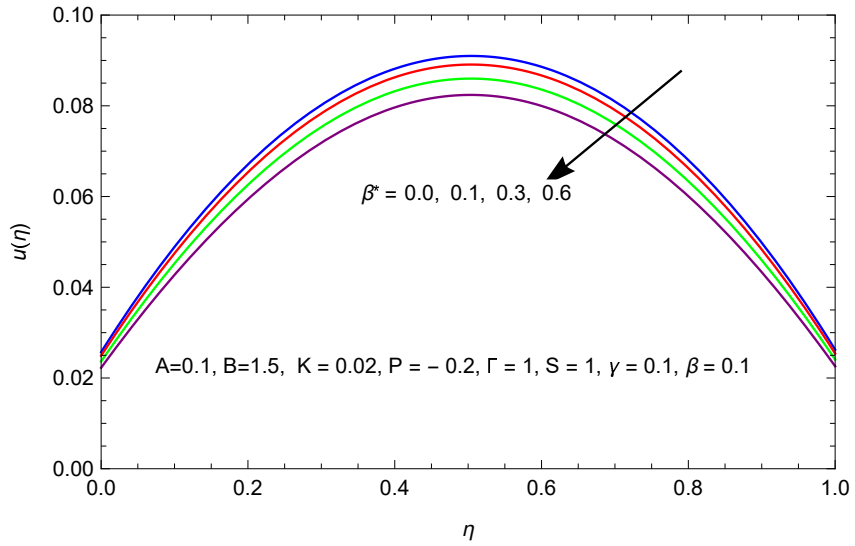

Figure 4: Velocity profile for β^*.

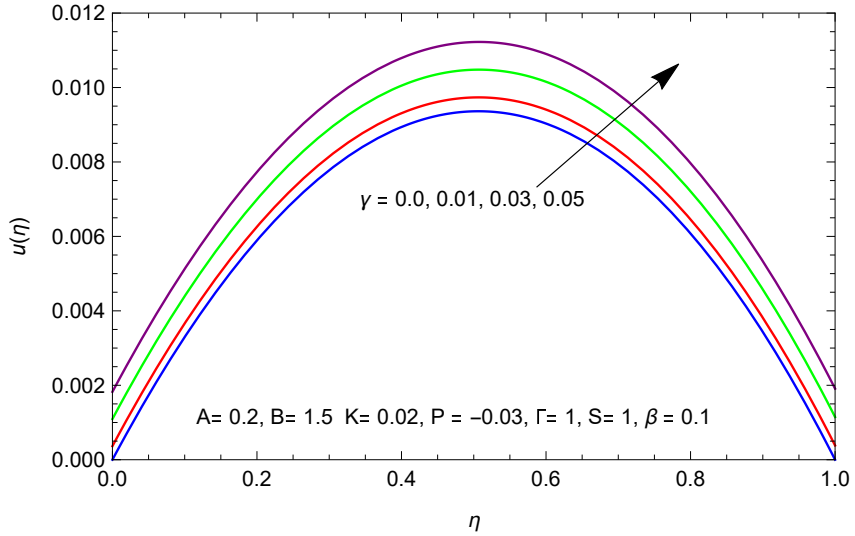

Figure 5: Velocity profile for γ.

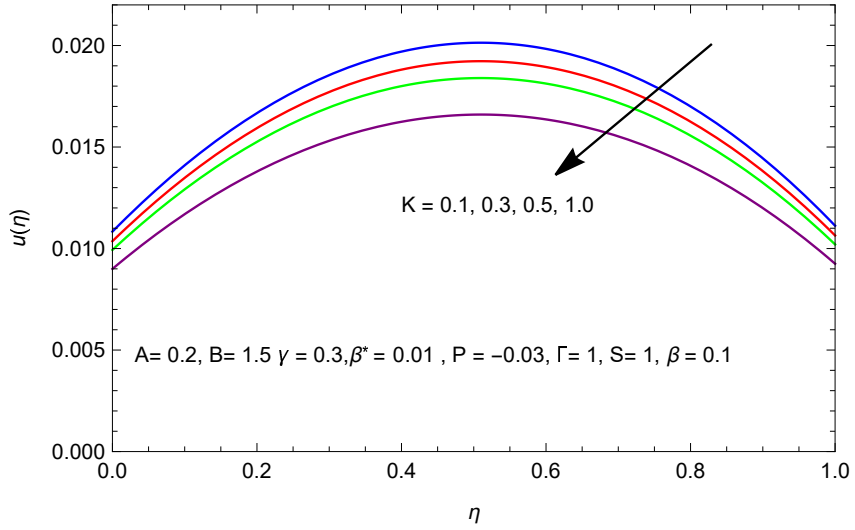

Figure 6: Velocity profile for K.

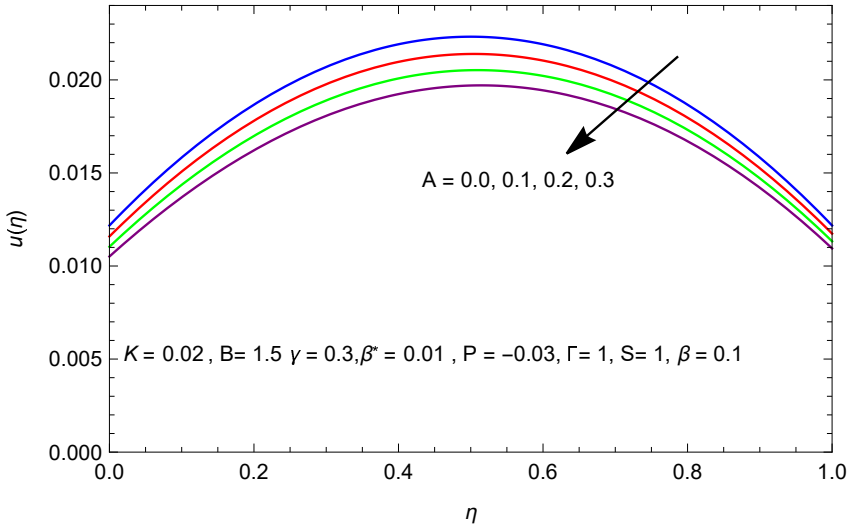

Figure 7: Velocity profile for A.

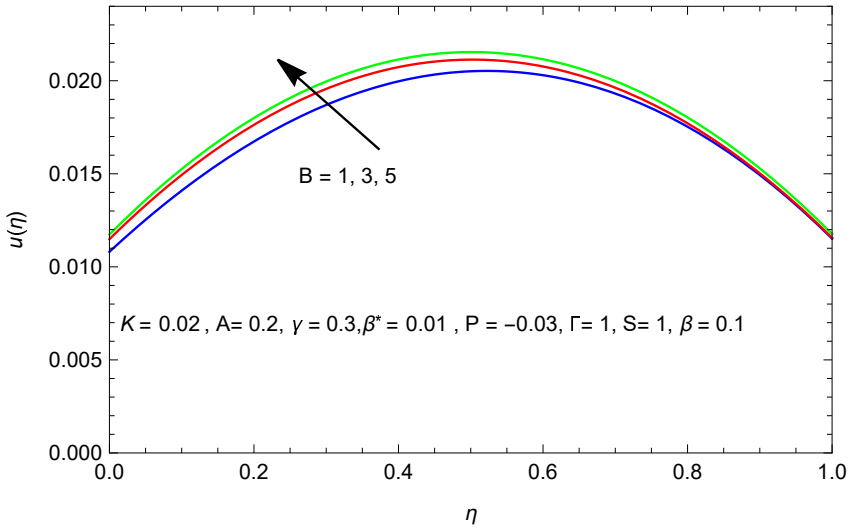

Figure 8: Velocity profile for B.

Figures 9–11 show temperature distribution $\theta(\eta)$ for assorted values of pertinent parameters. The influence of temperature jump parameter (β) is noticed to rise the temperature distribution (**Figure 9**). Physically, upsurge in temperature jump parameter (β) value implies increase in fluid temperature nearer to the walls (walls are kept at constant temperatures) and as a result, fluid temperature enhances. The Impact of internal heat source parameter (S) is depicted by **Figure 10**. It is seen in the graph that temperature field enhances with rise in value of S. The reason behind is that because temperature is a measure of heat, rise in heat source parameter (S) value enhances heat energy which causes increase in fluid temperature. Increasing value of Brinkman number (Γ) increases the fluid temperature because Γ is a parameter for frictional heating and more frictional heating causes increase in fluid temperature distribution (**Figure 11**).

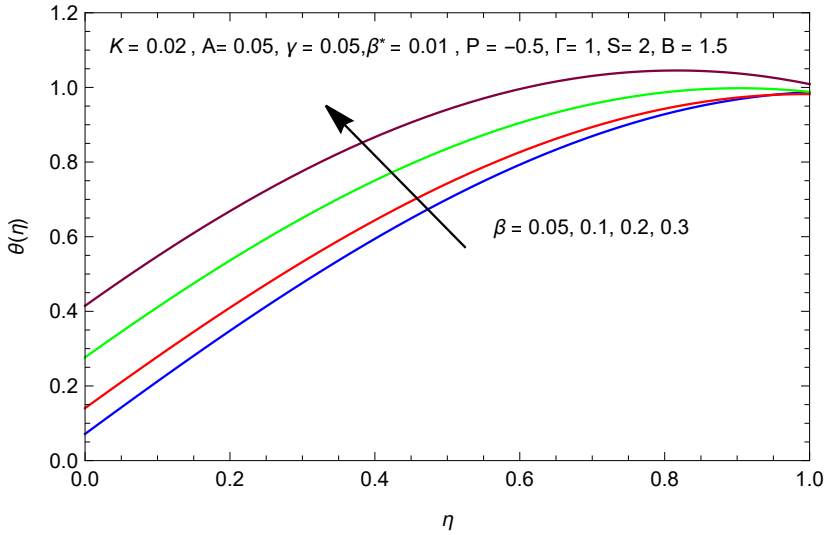

Figure 9: Tempreture profile for β.

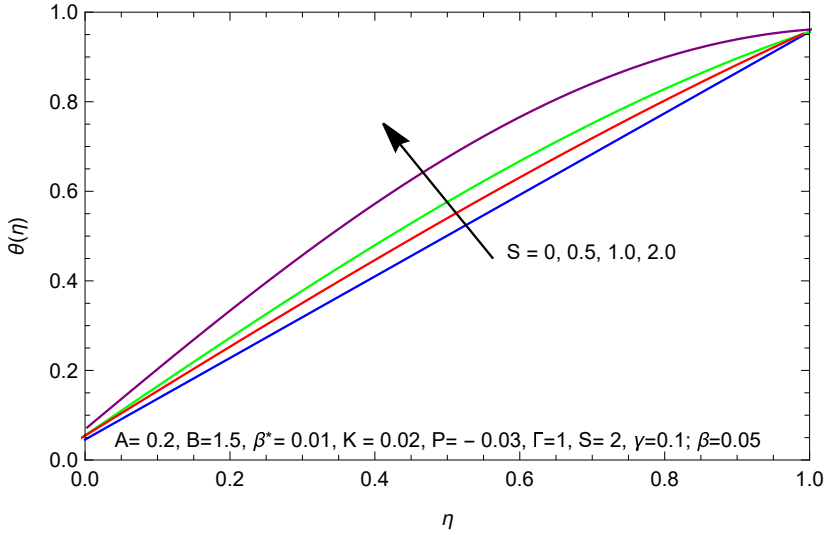

Figure 10: Tempreture profile for S.

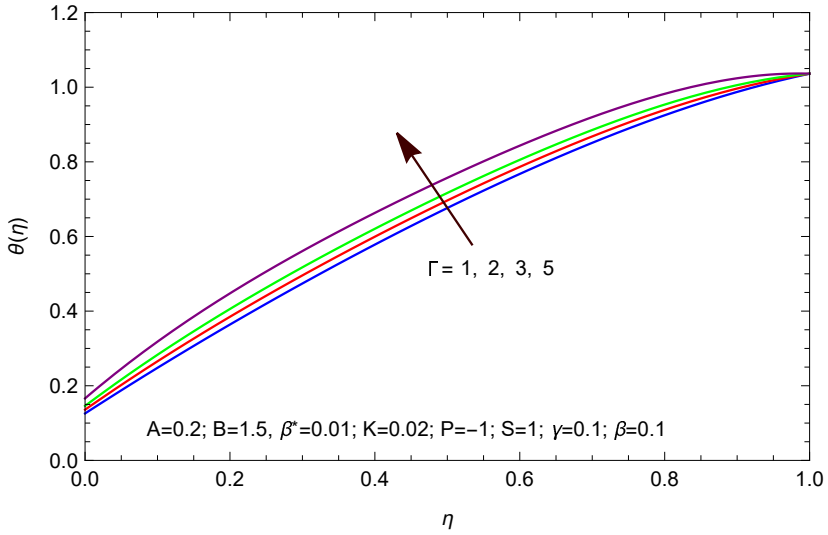

Figure 11: Tempreture profile for Γ.

Figures 12–17 depict variation in total entropy generation number (NS) for several values of arising physical parameters. The figures reveal that total entropy production number (NS) is maximum at the lower channel wall. NS decreases by increasing value of temperature slip parameter (β) in the entire channel width (**Figure 12**). Physically, with rising value of β fluid temperature enhances which causes reduction in NS. Impact of Brinkman number (Γ) is observed to enhance NS. It happens due to an increase in fluid friction with rising value of Γ. The effect is apparent near the walls, the reason behind is occurrence of higher velocity and temperature gradients in the region close to the walls whereas, in middle part of the channel no significant change is observed (**Figure 13**). Further, we noticed in **Figure 14** that enhancement in value of Vogel's viscosity parameter A causes reduction in NS while reverse effect is noticed due to rise in value of B (**Figure 15**). Further, we have seen that the ascending value of velocity slip parameter (γ) causes reduction in NS (**Figure 16**). Increasing value of heat generation parameter (S) increase NS in lower portion of the channel and reduce it in upper region (**Figure 17**).

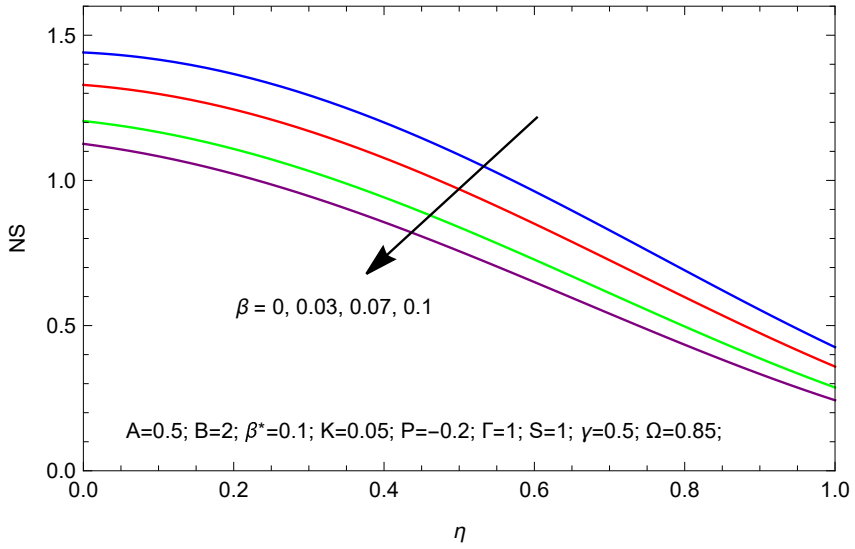

Figure 12: Entropy profile for β.

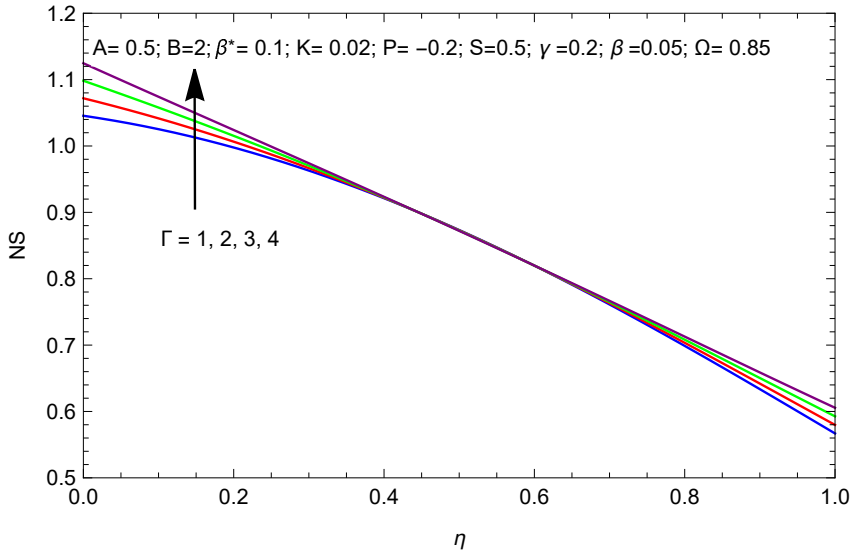

Figure 13: Entropy profile for Γ.

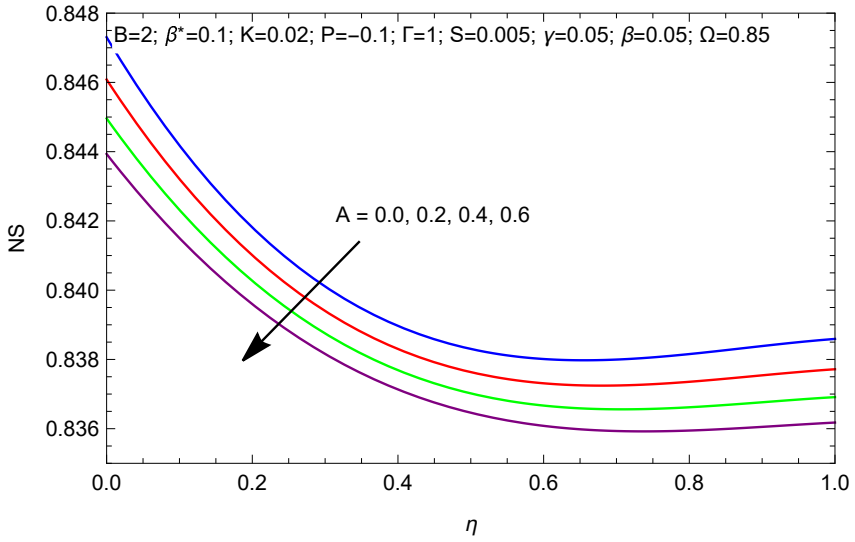

Figure 14: Entropy profile for A.

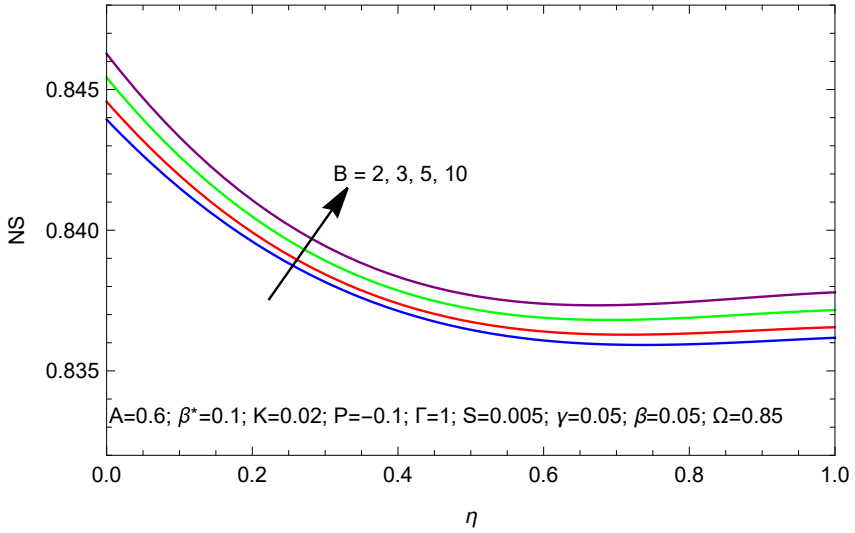

Figure 15: Entropy profile for B.

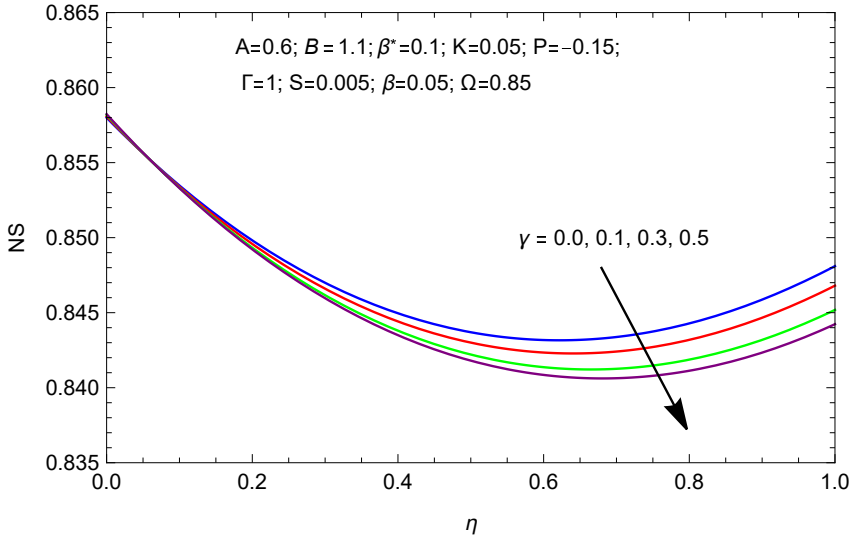

Figure 16: Entropy profile for γ.

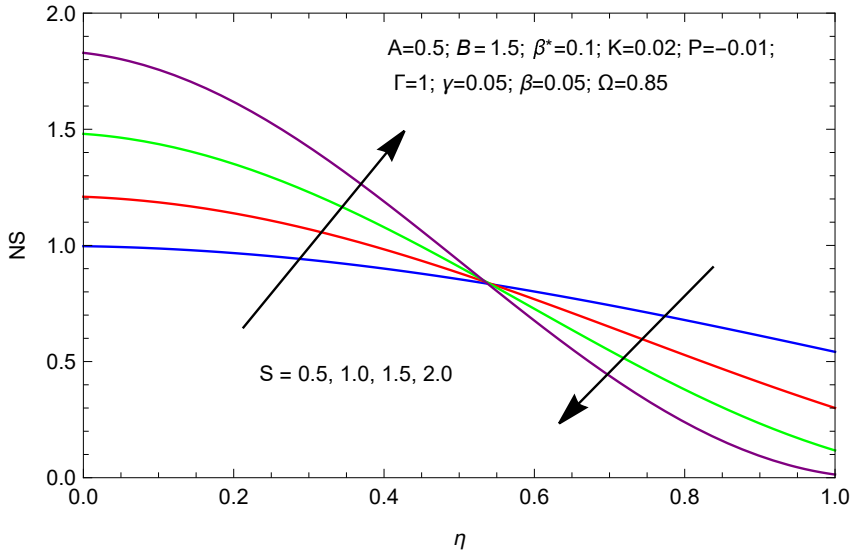

Figure 17: Entropy profile for S.

Figures 18–23 delineate variations in Bejan number (Be) for numerous values of pertinent parameters. These figures reveal that Bejan number attains a value close to its maximum value $(0 \leq Be \leq 1)$ in middle part of the channel. The reason behind is that as maximum velocity occurs in central part of the channel that is velocity gradient vanish in middle part of the channel which means that in central part of the channel entropy production due to fluid friction (NS_2) is negligible and hence Bejan number attains value close to its maximum value in this part. It is observed that upsurge in β value reduces Be and effect is more apparent in upper part, while Be decreases by an increase in parameter Γ value. Influence of Vogel's parameter A is noticed to rise Be, whereas reverse effect due to Vogel's parameter B is depicted. Influence of velocity slip parameter (γ) is seen to suppress Be in lower region, while it rises in upper part of the channel. Be also reduces with upsurging value of S in the region nearer to upper wall, while in rest part it attains value nearly its maximum value $(0 \leq Be \leq 1)$ which shows negligible entropy production due to viscous dissipation in the channel except the nearer region of the upper wall.

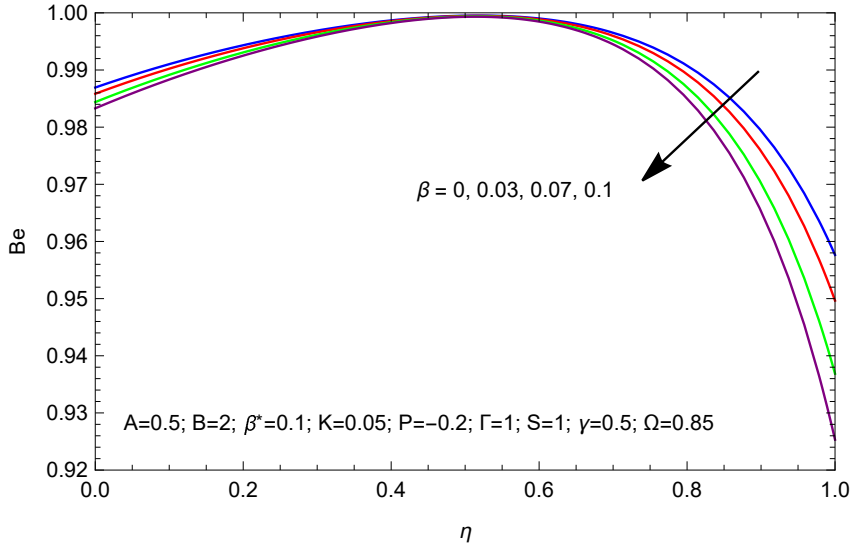

Figure 18: Bejan number for β.

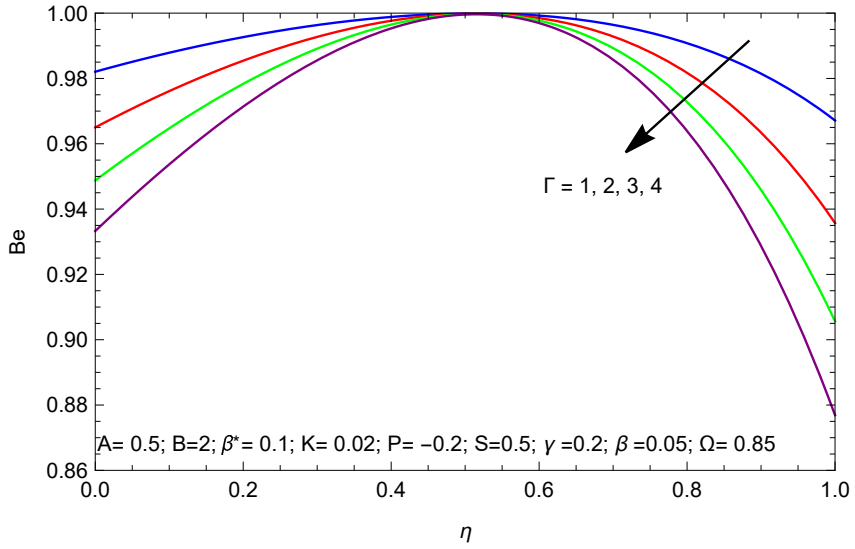

Figure 19: Bejan number for Γ.

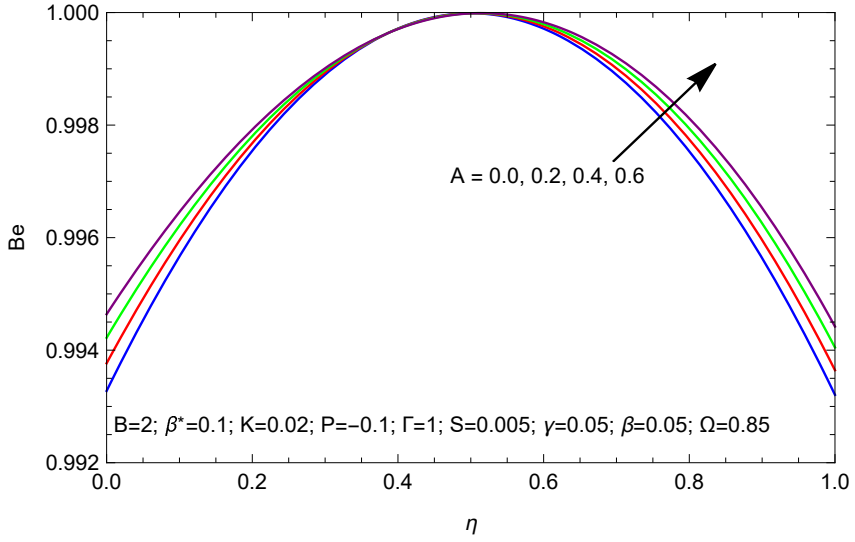

Figure 20: Bejan number for A.

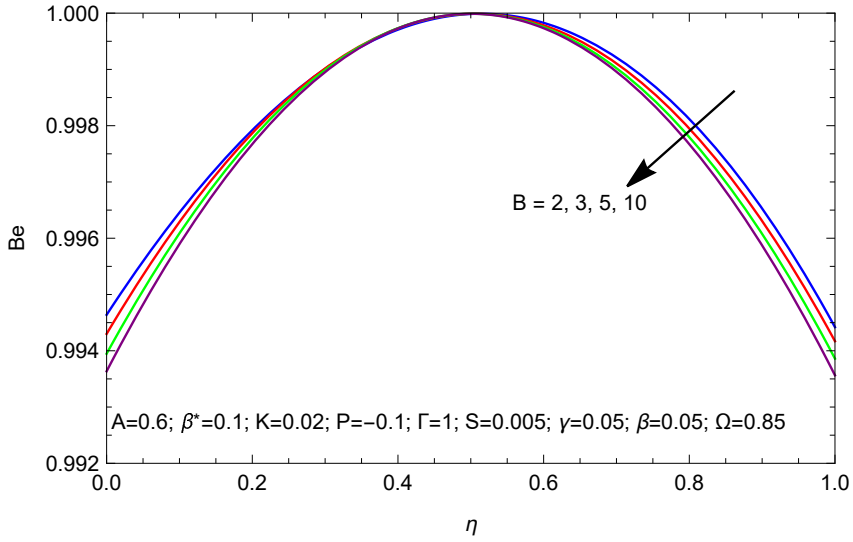

Figure 21: Bejan number for B.

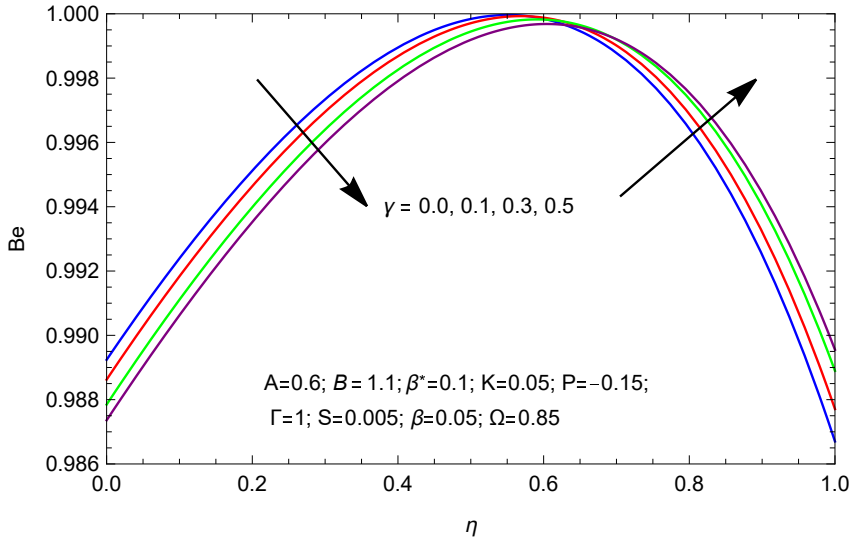

Figure 22: Bejan number for γ.

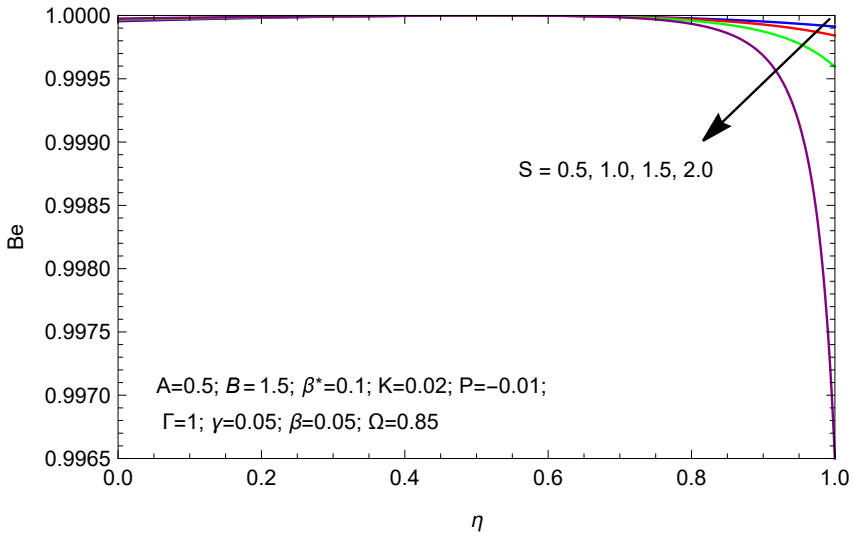

Figure 23: Bejan number for S.

In **Table 1** the values of velocity and temperature computed for particular values of parameters are compared with those obtained by Akinshilo [26] and found in excellent agreement.

Table 1: Comparison of velocity $u(\eta)$ and temperature $\theta(\eta)$ values, for $A = 0.1$, $B = 2.0$, $\Gamma = 1$, $\beta^* = 0.01$, $K = 0.01$, $P = -0.1$, $\theta_w = 1$, $\mu_* = 1$, $\gamma = 0$, $\beta = 0$, $S = 0$.

	$u(\eta)$		$\theta(\eta)$	
η	**Akinshilo[26]**	**Present study(HAM)**	**Akinshilo[26]**	**Present study(HAM)**
0.00	0	0	0	0
0.05	0.0062	0.00616250	0.0500	0.05004686
0.10	0.0117	0.01168653	0.1000	0.10008049
0.15	0.0166	0.01657034	0.1500	0.15010365
0.20	0.0208	0.02081219	0.2000	0.20011876
0.25	0.0244	0.02441036	0.2501	0.25012792
0.30	0.0274	0.02736313	0.3001	0.30013294
0.35	0.0297	0.02966880	0.3501	0.35013527
0.40	0.0313	0.03132566	0.4001	0.40013607
0.45	0.0323	0.03233203	0.4501	0.45013616
0.50	0.0327	0.03268623	0.5001	0.50013605
0.55	0.0324	0.03238661	0.5501	0.55013591
0.60	0.0314	0.03143151	0.6001	0.60013560
0.65	0.0298	0.02981929	0.6501	0.65013463
0.70	0.0275	0.02754833	0.7001	0.70013220
0.75	0.0246	0.02461702	0.7501	0.75012717
0.80	0.0210	0.02102376	0.8000	0.80011807
0.85	0.0168	0.01676699	0.8500	0.85010311
0.90	0.0118	0.01184513	0.9000	0.90008015
0.95	0.0063	0.00625664	0.9500	0.95004671
1.00	0	0	1	1

In **Table 2** values of skin friction coefficient at lower wall, $(C_f)_{\eta=0}$ and Nusselt number, (Nu) are presented for various values of the parameters. We noticed, $(C_f)_{\eta=0}$ lessens with increasing values of the parameters (B) and (K) while, the effect of parameters (A) and (γ) is found to upsurge it. The force exerted by moving fluid on the wall increases with enhancement in value of γ and as a result $(C_f)_{\eta=0}$ upsurges. Further, observed that increase in values of parameters (S) and (Γ) cause upsurge in Nusselt number (Nu) in the absolute sense however, the temperature slip parameter (β) reduces it. The negative sign in Nu values shows that heat transfer takes place from fluid towards the wall.

Table 2: Skin-friction coefficient and Nusselt number values, when $P = -0.01$, $\beta^* = 0.01$.

A	B	K	γ	β	Γ	S	$(C_f)_{\eta=0}$	Nu
0.2	2.0	0.01	0.01	0.01	1.0	1.0	0.005039	–1.169398
0							0.004995	–1.169408
0.2							0.005039	–1.169398
0.4							0.005086	–1.169389
	2.0						0.005039	–1.169398
	3.0						0.005014	–1.169400
	4.0						0.005006	–1.169402
		0.0					0.005044	–1.169399
		0.5					0.004831	–1.169391
		1.0					0.004639	–1.169385
			0.0				0.005038	
			0.1				0.005049	
			0.3				0.005061	
				0.0				–1.188406
				0.05				–1.099838
				0.1				–1.025073
					1			–1.169398
					2			–1.169410
					5			–1.169443
						0.5		–1.069096
						1.0		–1.169398
						2.0		–1.414729

Conclusions

In this research, analytical investigation of entropy generation in non-Newtonian third-grade flow along with heat transport has been carried out. The flow is assumed to take place in a parallel-plate channel via porous medium. Impacts of numerous occurring physical parameters on velocity distribution, temperature, entropy production along with Bejan number are exhibited by plots and discussed. The outcomes of the study are outlined as follow: (1) Velocity slip parameter (γ) substantially enhances the fluid flow while non-Newtonian parameter (β^*) and porous medium parameter (K) reduce it; (2) Influence of heat generation parameter (S) and Brinkman number (Γ) is noticed to increase the temperature distribution. Temperature distribution also increases with rising temperature slip (β); (3) Maximum entropy production noticed near the lower wall; (4) NS lessens with upsurge in values of γ and β; (5) Influence of S is noticed to enhance entropy generation in lower channel part while reverse trend is observed in upper channel part; (6) Bejan number attains maximum value $(0 \leq Be \leq 1)$ in middle of the channel and decreases with rising value of β, Γ and S; (7) Effect of γ is noticed to upsurge $(C_f)_{\eta=0}$; (8) Effect of β is seen to reduce Nu in the absolute sense; (9) The parameters (A, B) exhibit opposite impacts on velocity, entropy generation and Bejan

number.

Acknowledgements

The support provided by CSIR, and UGC through Senior Research Fellowship to Mukesh Kumar and Rahul Choudhary, respectively are gratefully acknowledged.

References

[1] A Bejan. *Convection heat transfer.* 3rd ed. Wiley, New Jersey, 2004.

[2] A Bejan. A study of entropy generation in fundamental convective heat transfer. *J. Heat Tran.* 1979; **101**, 718-25.

[3] A Bejan. *Entropy generation minimization*, CRC Press, Florida, 1996.

[4] DS Chauhan and V Kumar. Entropy analysis for third-grade fluid flow with temperature-dependent viscosity in annulus partially filled with porous medium. *Theor. Appl. Mech.* 2013; **40**, 441-64.

[5] SO Adesanya and JA Falade. Thermodynamics analysis of hydromagnetic third grade flow through a channel filled with porous medium. *Alexandria Eng. J.* 2015; **54**, 615-22.

[6] MG Sobamowo and AT Akinshilo. Analysis of flow, heat transfer and entropy generation in a pipe conveying fourth grade fluid with temperature-dependent viscosities and internal heat generation. *J. Mol. Liq.* 2017; **241**, 188-98.

[7] K Madhavi, VR Prasad, SA Gaffar and V Kothuru. Entropy analysis of third-grade MHD convection flows from a horizontal cylinder with slip. *Arch. Mech. Eng.* 2018; **65**, 417-40.

[8] M Madhu, NS Shashikumar, B Mahanthesh, BJ Gireesha and N Kishan. Heat transfer and entropy generation analysis of non-Newtonian fluid flow through vertical microchannel with convective boundary condition. *Appl. Math. Mech.* 2019; **40**, 1285-300.

[9] R Zhang, S Aghakhani, A Hazatzadeh Pordanjani, SM Vahedi, A Shahsavar and M Afrand. Investigation of the entropy generation during natural convection of Newtonian and non-Newtonian fluids inside the L-shaped cavity subjected to magnetic field: application of lattice Boltzmann method. *Eur. Phys. J. Plus* 2020; **135**, 184.

[10] NS Shashikumar, K Triveni, M Madhu, B Mahantesh, BJ Gireesha and N Kishan. Entropy generation analysis of radiative Williamson fluid flow in an inclined microchannel with multiple slip and convective heating boundary effects. *Proc. IME. E J. Process Mech. Eng.* 2021, https://doi.org/10.1177/095440892110498.

[11] P Vyas, S Khan and Gajanand. Thermo-fluidics and entropy generation analysis of couple stress Casson fluid in a channel with stretching walls. *Int. J. Ambient Energ.* 2022; **43**, 8206-19.

[12] RL Fosdick and KR Rajagopal. Thermodynamics and stability of fluids of third grade. *Proc. Roy. Soc. Lond. Math. Phys. Sci.* 1980; **369**, 351-77.

[13] M Massoudi and I Christie. Effects of variable viscosity and viscous dissipation on the flow of a third grade fluid in a pipe. *Int. J. Non Lin. Mech.* 1995; **30**, 687-99.

[14] PD Ariel. Flow of a third grade fluid through a porous flat channel. *Int. J. Eng. Sci.* 2003; **41**, 1267-85.

[15] N Ali, Y Wang, T Hayat and M Oberlack. Slip effects on the peristaltic flow of a third grade fluid in a circular tube. *J. Appl. Mech.* 2009; **76**, 011006.

[16] M Yurusoy, M Pakdemirli and BS Yilbas. Perturbation solution for third-grade fluid flowing between parallel plates. *Proc. Inst. Mech. Eng. C Mech. Eng. Sci.* 2008; **222**, 653-6.

[17] R Ellahi, T Hayat, FM Mohmed and S Asghar. Effects of slip on the nonlinear flow of the third grade fluid. *Nonlinear Anal. R. World Appl.* 2010; **11**, 139-46.

[18] T Hayat, M Mustafa and S Asghar. Unsteady flow with heat and mass transfer of a third grade fluid over a stretching surface in the presence of chemical reaction. *Nonlinear Anal. R. World Appl.* 2010; **11**, 3186-97.

[19] AW Ogunsola and B. A. Peter. Effect of variable viscosity on third grade fluid flow over a radiative surface with Arrhenius reaction. *Int. J. Pure Appl. Sci. Tech.* 2014; **22**, 1-8.

[20] BY Ogunmola, AT Akinshilo and MG Sobamowo. Perturbation solutions for Hagen-Poiseuille flow and heat transfer of third grade fluid with temperature-dependent viscosities and internal heat generation. *Int. J. Eng. Math.* 2016; **2016**, 8915745.

[21] AA Khan, SR Bukhari, M Matrin and R Ellahi. Effects of chemical reaction on third grade MHD fluid flow over a stretching surface under the influence of heat and mass transfer with variable reactive index. *Heat Tran. Res.* 2018; **50**, 1061-80.

[22] Y Aksoy and M Pakdemirli. Approximate analytical solutions for flow of a third-grade fluid through a parallel-plate channel filled with a porous medium. *Transport Porous Media* 2010; **83**, 375-95.

[23] T Hayat, R Naz and S Abbasbandy. Poiseuille flow of a third-grade fluid in porous medium. *Transport Porous Media* 2011; **87**, 355-66.

[24] IG Baoku, BI Olajuwo and AO Mustapha. Heat and mass transfer on a MHD third grade fluid with partial slip flow past an infinite vertical insulated porous plate in a porous medium. *Int. J. Heat Fluid Flow* 2013; **40**, 81-8.

[25] KV Prasad, SA Gaffar, EK Reddy and OA Beg. Numerical study of non-Newtonian boundary layer flow of Jeffreys fluid past a vertical porous plate in a non-Darcy porous medium, *Int. J. Comput. Meth. Eng. Sci. Mech.* 2014; **15**, 372-89.

[26] AT Akinshilo. Steady flow and heat transfer analysis of third grade fluid with porous medium and heat generation. *Eng. Sci. Tech. Int. J.* 2017; **20**, 1602-9.

[27] F Ahmed and M Iqbal. MHD power law fluid flow and heat transfer analysis through Darcy Brinkman porous media in annular sector. *Int. J. Mech. Sci.* 2017; **130**, 508-17.

[28] P Maghsoudi, G Shahriari, M Mirzaei and M Mirzei. Natural convection of third-grade non-Newtonian fluid flow in a porous medium with heart source: analytical solution. *Eur. Phys. J. Plus* 2018; **133**, 502.

[29] L Rundora and OD Makinde. Unsteady MHD flow of non-Newtonian fluid in a channel filled with a saturated porous medium with asymmetric Navier slip and convective heating. *Appl. Math. Inform. Sci.* 2018; **12**, 483-93.

[30] KP Priyadarsan and S Panda. Heat transfer in unsteady magnetohydrodynamic flow of fourth-grade fluid through a porous medium between two infinite parallel plates with time dependent suction. *Spec. Top. Rev. Porous Media* 2020; **11**, 239-58.

[31] A Olkha and A Dadheech. Second law analysis for Casson fluid flow over permeable surface embedded in porous medium. *Nonlinear Stud.* 2021; **28**, 1271-85.

[32] A Olkha and A Dadheech. Second law analysis for radiative magnetohydrodynamic slip flow for two different non-Newtonian fluids with heat source. *J. Nanofluids* 2021; **10**, 447-61.

[33] A Olkha and M Kumar. Casson fluid flow in a vertical annulus through porous medium with heat transfer characteristics and chemical reaction: An exact solution. *Int. J. Mod. Phys. C* 2022; **34**, 2350078.

[34] SJ Liao. 1992, The proposed homotopy analysis technique for the solution of nonlinear problems. Ph. D. Dissertation. Shanghai Jiao Tong University, Shanghai, China.

[35] S Liao. *Beyond perturbation: introduction to the homotopy analysis method.* Chapman and Hall, Florida, 2003.

[36] S Liao and Y Tan. A general approach to obtain series solutions of nonlinear differential equations. *Stud. Appl. Math.* 2007; **119**, 297-354.

[37] JB Anasuya and S Srinivas. Heat transfer characteristics of magnetohydrodynamic two fluid oscillatory flow in an inclined channel with saturated porous medium. *Proc. IME. E J. Process Mech. Eng.* 2023, https://doi.org/10.1177/09544089221146364.

[38] S Maatoug, HK Babu, VVL Deepti, K Ghachem, K Raghunatth, C Ganteda and SM Khan. Variable chemical species and thermo-diffusion Darcy-Forchheimer squeezed flow of Jeffery nanofluid in horizontal channel with viscous dissipation effects. *J. Indian Chem. Soc.* 2023; **100**, 100831.

[39] A Ganjikunta, HK Babu, V Bhajanthri and R Kodi. An unsteady MHD flow of a second-grade fluid passing through a porous medium in the presence of radiation absorption exhibits Hall and ion slip effects. *Heat Tran.* 2022; **52**, 780-806.

[40] OT Bafakeeh, K Raghunath, F Ali, M Khalid and SM Eldin. Hall current and soret effects on unsteady MHD rotating flow of second-grade fluid through porous media under the influence of thermal radiation and chemical reactions. *Catalysts* 2022; **12**, 1233.

[41] K Raghunath and R Mohanaramana. Hall, soret, and rotational effects on unsteady MHD rotating flow of a second-grade fluid through a porous medium in the presence of chemical reaction and aligned magnetic field. *Int. Comm. Heat Mass Tran.* 2022; **137**, 106287.

[42] VVL Deepthi, MMA Lashin, NR Kumar, K Raghunath, F Ali, M Oreijah, K Guedri, SM Eldin, MI Khan and AM Galal. Recent development of heat and mass transport in the presence of hall, ion slip and thermo diffusion in radiative second grade material: Application of micro machines. *Micromachines* 2022; **13**, 1566.

[43] R Kodi and M Ravuri. *Soret and chemical reaction effects on heat and mass transfer in MHD flow of a Kuvshinski fluid through porous medium with aligned magnetic field and radiation.* Nonlinear dynamics and applications. Springer, Switzerland, 2022, p. 377-91.

[44] MP Devi and S Srinivas. Two layered flow of viscoelastic liquid in a vertical porous channel with hall current, thermal radiation and chemical reaction. *Int. Comm. Heat Mass Tran.* 2023; **142**, 106612.

[45] YS Kumar, S Hussain, K Raghunath, F Ali, K Guedri, SM Eldin and ML Khan. Numerical analysis of magnetohydrodynamics Casson nanofluid flow with activation energy, Hall current and thermal radiation. *Sci. Rep.* 2023; **13**, 4021.

[46] S Li, K Raghunath, A Alfaleh, F Ali, A Zaib, MI Khan, SM Eldin and V Puneeth. Effects of activation energy and chemical reaction on unsteady MHD dissipative Darcy-Forchheimer squeezed flow of Casson fluid over horizontal channel. *Sci. Rep.* 2023; **13**, 2666.

[47] R Kodi, C Ganteda, A Dasore, ML Kumar, G Laxmaiah, MA Hasan, S Islam and A Razak. Influence of MHD mixed convection flow for Maxwell nanofluid through a vertical cone with porous material in the existence of variable heat conductivity and diffusion. *Case Stud. Therm. Eng.* 2023; **44**, 102875.